Coupled Multi-Robot Systems Under Linear Temporal Logic and Signal Temporal Logic Tasks

Lars Lindemann, *Student Member, IEEE*, Jakub Nowak, Lukas Schönbächler, Meng Guo, *Member, IEEE*, Jana Tumova, *Member, IEEE*, and Dimos V. Dimarogonas, *Senior Member, IEEE*

***Abstract*— This brief presents the implementation and experimental results of two frameworks for multi-agent systems under temporal logic tasks, which we have recently proposed. Each agent is subject to either a local linear temporal logic (LTL) or a local signal temporal logic (STL) task where each task may further be coupled, i.e., the satisfaction of a task may depend on more than one agent. The agents are represented by mobile robots with different sensing and actuation capabilities. We propose to combine the two aforementioned frameworks to use the strengths of both LTL and STL. For the implementation, we take into account practical issues, such as collision avoidance, and, in particular, for the STL framework, input saturation, the digital implementation of continuous-time feedback control laws, and a controllability assumption that was made in the original work. The experimental results contain three scenarios that show a wide variety of tasks.**

***Index Terms*— Autonomous mobile robots, decentralized robotic networks, formal methods-based control synthesis, linear temporal logic (LTL), signal temporal logic (STL).**

I. Introduction

A MULTI-AGENT system is a collection of independent agents with the goal to achieve global or local (individual) tasks. Collaborative control deals with achieving global tasks, such as consensus [1], formation control [2], connectivity maintenance [3], and collision avoidance [4], see also [5] for an overview. To impose more complex tasks, such as recurrence, request–response, and time-constrained tasks, ideas from formal verification [6] have been used where the tasks are written as temporal logic formulas. Control methods for systems under temporal logic tasks can be seen as multipurpose tools and are, hence, of high interest for practical applications, i.e., tasks can easily be changed while automatically obtaining correct-by-design controllers. Linear temporal logic (LTL) is a proposition-based logic used for single-agent systems [7]–[12] and for multi-agent systems [13]–[18] where, especially for multi-agent systems, the computational complexity is known to be high. LTL tasks can include combinations of surveillance ("periodically visit regions A, B, and C"), safety ("always avoid region D"), and many others. Signal temporal logic (STL) is a predicate-based logic interpreted over continuous-time signals [19]. STL entails space robustness [20], a form of the robust semantics [21], stating how robustly a signal satisfies a temporal logic formula. Control synthesis under STL tasks has been considered for single-agent systems [22]–[30] and for multi-agent systems [31], [32]. A common tradeoff is to find a restricted, yet expressive STL fragment that allows for computationally efficient control as in [25] and [31]. STL tasks can again include combinations of surveillance ("visit regions A, B, and C every 10–60 s while agents form a triangular formation"), safety ("always between 5 and 25 s stay at least 1 m away from D"), and many others. Compared with LTL, STL now allows to impose the desired quantitative temporal and spatial properties on the system. Multi-agent systems under temporal logic tasks are separated into two classes: top-down and bottom-up. In the former, a global task is assigned to the team of agents, while in the latter, each agent is subject to a local (individual) task regardless of what other agents are assigned. These local tasks may be coupled, i.e., the satisfaction of a local task may depend on the behavior of other agents. Top-down approaches usually resort to decomposing the global task into local ones. We argue, hence, that a bottom-up approach is more general and considered here.

We consider a heterogenous multi-agent system consisting of mobile robots, as shown in Fig. 1. Each robot is subject to either a local LTL or a local STL task. Our main contribution is the implementation and experimental results of the frameworks [14] and [31] to demonstrate the advantages of the computationally efficient and robust methods presented therein. To account for the computational burdens of the LTL plan synthesis, poses of interest are considered in [14] for the abstraction of the workspace, while the approach for STL control synthesis in [31] is inherently computationally efficient due to the use of time-varying feedback control laws. We also aim at demonstrating the practical advantages of using both LTL and STL at the same time. Note that STL is a more

Manuscript received August 24, 2019; accepted October 30, 2019. Date of publication December 27, 2019; date of current version February 9, 2021. Manuscript received in final form November 20, 2019. This work was supported in part by the Swedish Research Council (VR), in part by the European Research Council, in part by the Swedish Foundation for Strategic Research, in part by the EU H2020 Co4Robots Project, and in part by the Knut and Alice Wallenberg Foundation. Recommended by Associate Editor G. Hu. *(Corresponding author: Lars Lindemann.)*

L. Lindemann, J. Nowak, and D. V. Dimarogonas are with the Division of Decision and Control Systems, KTH Royal Institute of Technology, 10044 Stockholm, Sweden (e-mail: llindem@kth.se; jakubn@kth.se; dimos@kth.se).

L. Schönbächler is with Bucher Hydraulics, 6345 Neuheim, Switzerland (e-mail: luki.schoenb@hotmail.de).

M. Guo is with the Bosch Center for Artificial Intelligence, 71272 Renningen, Germany (e-mail: meng.guo2@de.bosch.com).

J. Tumova is with the Division of Robotics, Perception, and Learning, KTH Royal Institute of Technology, 10044 Stockholm, Sweden (e-mail: tumova@kth.se).

Color versions of one or more of the figures in this article are available online at https://ieeexplore.ieee.org.

Digital Object Identifier 10.1109/TCST.2019.2955628

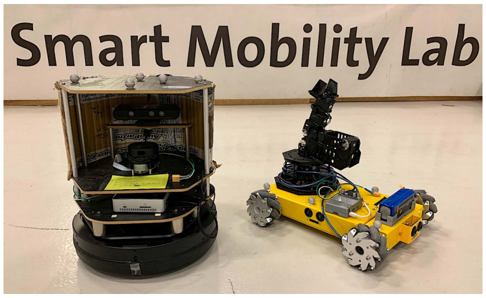

Fig. 1. TurtleBots (left) and Nexus 4WD Mecanum Robotic Cars (right) are used in the experiments in Section IV.

complex task specification language than LTL. In fact, STL allows to impose timed tasks, such as strict deadlines, while admitting predicates as opposed to simple propositions in LTL. For multi-agent systems, this implies that predicates can be used to couple agents with each other in a straightforward manner. Control approaches for LTL are mature and allow to use the full LTL fragment while STL control methods are still being investigated, currently only with results for fragments of STL [25], [31]. Existing methods for the full STL fragment [22], [28] discretize time (hence, are, in some sense, equivalent to LTL) and are computationally demanding. We propose to use STL when timed tasks or tasks involving the coupling of agents are of interest while, otherwise, methods for LTL can be used. One of the emerging features is the following: the STL fragment in [31] does not allow to specify periodic tasks, but by coupling an agent, by means of an STL task, to agents under LTL tasks, periodic, and complex behaviors can be induced. Agents also need to avoid collisions so that both dynamical and task level couplings are present.

Section II summarizes [14] and [31], while Section III describes our implementation. Experimental results are shown in Section IV, followed by conclusions in Section V.

II. Preliminaries

Let $\mathbb{R}^n$ be the n-dimensional real vector space. The set of real and non-negative real numbers are $\mathbb{R}$ and $\mathbb{R}_{\geq 0}$, respectively, and $\mathbf{0}_n$ is a vector containing n zeros.

Consider M agents where $M_{\text{LTL}} \leq M$ agents are subject to local LTL tasks, while $M_{\text{STL}} := M - M_{\text{LTL}}$ agents are subject to local STL tasks. Each agent i is described by three states $x_{i,1}$, $x_{i,2}$, and $x_{i,3}$, where $x_{i,1}$ and $x_{i,2}$ describe the agent's 2-D position, while $x_{i,3}$ describes the agent's orientation with respect to the x_1-axis. Let $\boldsymbol{x}_i := [z_i^T \;\; x_{i,3}]^T \in \mathcal{X} \subseteq \mathbb{R}^3$ where $z_i := [x_{i,1} \;\; x_{i,2}]^T$ and $\mathcal{X}$ is the workspace. We model each agent $i \in \{1, \ldots, M\}$ by

$$\dot{\boldsymbol{x}}_i(t) = f_i(\boldsymbol{x}_i(t)) + g_i(\boldsymbol{x}_i(t))\boldsymbol{u}_i(t) + \boldsymbol{w}_i(t) \qquad (1)$$

where $\boldsymbol{u}_i \in \mathbb{R}^{m_i}$ and $\boldsymbol{w}_i \in \mathbb{R}^3$ are the control input and additive disturbance, respectively. Furthermore, define $\boldsymbol{x} := [\boldsymbol{x}_1{}^T \;\; \ldots \;\; \boldsymbol{x}_M{}^T]^T$. The multi-agent system is modeled by an undirected graph $\mathcal{G} := (\mathcal{V}, \mathcal{E})$ [5]. The set of agents is $\mathcal{V} := \{1, 2, \ldots, M\}$, while the edge set $\mathcal{E} \in \mathcal{V} \times \mathcal{V}$ indicates communication links. We define the *behavior* of agent i to be agent i's trajectory, i.e., the solution $\boldsymbol{x}_i : \mathbb{R}_{\geq 0} \to \mathbb{R}^3$ to (1).

A. Linear Temporal Logic

For each $i \in \{1, \ldots, M_{\text{LTL}}\}$, consider the set of atomic propositions AP_i; $\alpha_i \in AP_i$ can either be true ($\top$) or false ($\bot$) and, for instance, indicate whether or not an agent is in a certain region or performing a certain action. We assume that the satisfaction of α_i does only depend on the behavior of agent i. The set of LTL formulas is

$$\phi_i ::= \top \mid \alpha_i \mid \neg\phi_i \mid \circ\,\phi_i \mid \phi_i' \wedge \phi_i'' \mid \phi_i' \, U \, \phi_i'' \qquad (2)$$

where ϕ_i' and ϕ_i'' are LTL formulas associated with agent i and $\wedge$, $\neg$, $\circ$, and U denote the conjunction, negation, next, and until operators, respectively. The disjunction ($\vee$), eventually (F), and always (G) operators can be derived similarly [6]. An infinite *word* over the alphabet 2^{AP_i}, where 2^{AP_i} is the power set of AP_i, is an infinite sequence $\sigma_i := \sigma_{i,0}\sigma_{i,1}\sigma_{i,2}\cdots \in (2^{AP_i})^\omega$ where $\sigma_{i,k} \in 2^{AP_i}$ is the set of atomic propositions that are true at time step k. The semantics of LTL are given in [6, Definition 5.6] and stated as a relation $(\sigma_i, k) \models \phi_i$, which means that σ_i satisfies a formula ϕ_i at time step k. For instance, $(\sigma_i, 0) \models \phi_i$ with $\phi_i := G\neg\alpha_i' \wedge F\alpha_i''$ implies that $\forall k \geq 0$, $\alpha_i' \notin \sigma_{i,k}$ (α_i' is always avoided) and $\exists l \geq 0$ such that $\alpha_i'' \in \sigma_{i,l}$ (eventually α_i'' holds). The set of words that satisfy ϕ_i is given by $Words(\phi_i) := \{\sigma_i \in (2^{AP_i})^\omega | (\sigma_i, 0) \models \phi_i\}$. Each ϕ_i can be translated into a language equivalent Büchi Automaton $\mathcal{A}_{\phi_i} := (Q_i, 2^{AP_i}, \Delta_i, Q_{i,0}, \mathcal{F}_i)$ where Q_i is a finite set of states, $Q_{i,0} \subseteq Q_i$ is a set of initial states, 2^{AP_i} is the alphabet, $\Delta_i : Q_i \times 2^{AP_i} \to 2^{Q_i}$ is a transition relation, and $\mathcal{F}_i \subseteq Q_i$ is a set of accepting states. The sequence $q_i := q_{i,j_0}q_{i,j_1}q_{i,j_2}\cdots \in Q_i^\omega$ is a *run* of $\mathcal{A}_{\phi_i}$ for σ_i if $q_{i,j_0} \in Q_{i,0}$ and $\Delta_i(q_{i,j_k}, \sigma_{i,k}) = q_{i,j_{k+1}}$ for all $k \geq 0$. The run q_i is accepting if $q_{i,j_k} \in \mathcal{F}_i$ for infinitely many k. Let $\mathcal{L}_\omega(\mathcal{A}_{\phi_i}) := \{\sigma_i \in (2^{AP_i})^\omega | q_i$ is an accepting run of $\mathcal{A}_{\phi_i}$ for $\sigma_i\}$. There always exists a $\mathcal{A}_{\phi_i}$ with $Words(\phi_i) = \mathcal{L}_\omega(\mathcal{A}_{\phi_i})$ [6, Th. 5.41]. For more intuition on LTL and this terminology, we refer to [17, Ex. 1], [6, Section 5], and also the three experiments that we present in Section IV. Each agent $i \in \{1, \ldots, M_{\text{LTL}}\}$ has a set of propositions $\Pi_i \subseteq AP_i$ where $\alpha_{i,m} \in \Pi_i$ is associated with a set $\mathcal{X}_{i,m} \subseteq \mathbb{R}^3$ so that $\alpha_{i,m} = \top$ if $\boldsymbol{x}_i \in \mathcal{X}_{i,m}$. A transition from $\alpha_{i,m}$ to $\alpha_{i,n}$ is enabled if a navigation controller $\boldsymbol{u}_i$ exists that is able to drive the agent from any pose in $\mathcal{X}_{i,m}$ to some pose in $\mathcal{X}_{i,n}$ in finite time. Based on this, define a weighted finite-state transition system as a tuple $\mathcal{T}_i := (\Pi_i, \to_i, \Pi_{i,0}, L_i, W_i)$, where Π_i are the poses of interest, $\to_i \subseteq \Pi_i \times \Pi_i$ is the transition relation when there exists a navigation controller $\boldsymbol{u}_i$, $\Pi_{i,0} \subseteq \Pi_i$ is the set of initial regions, $L_i : \Pi_i \to 2^{AP_i}$ is the labeling function, and $W_i : \Pi_i \times \Pi_i \to \mathbb{R}_{\geq 0}$ is the weight function associated with a transition. Note that propositions in $AP_i \setminus \Pi_i$ are generic propositions that may hold for some poses of interest. We define an infinite *path* of $\mathcal{T}_i$ as an infinite state sequence $\tau_i = \pi_{i,j_0}\pi_{i,j_1}\ldots$ such that $\pi_{i,j_0} \in \Pi_{i,0}$ and a transition $\to_i$ exists from π_{i,j_k} to $\pi_{i,j_{k+1}}$ for all $k \geq 0$. A state sequence induces an infinite word $Word(\tau_i) = L_i(\pi_{i,j_0})L_i(\pi_{i,j_1})\ldots$. For a given formula ϕ_i and a path τ_i, we have that $(Word(\tau_i), 0) \models \phi_i$ if $Word(\tau_i) \in Words(\phi_i)$. A weighted product Büchi automaton, capturing the behavior of an agent that satisfies ϕ_i, is defined as $\mathcal{A}'_{\phi_i} := \mathcal{T}_i \times \mathcal{A}_{\phi_i} = (Q'_i, 2^{AP_i}, \Delta'_i, Q'_{i,0}, \mathcal{F}'_i, W'_i)$, where $Q'_i := \Pi_i \times Q_i, q'_i := \langle \pi_{i,m}, q_{i,o} \rangle \in Q'_i$, for all $\pi_{i,m} \in \Pi_i$ and for all $q_{i,o} \in Q_i$; $\Delta'_i : Q'_i \to 2^{Q'_i}$, $\langle \pi_{i,n}, q_{i,p} \rangle \in \Delta'_i(\langle \pi_{i,m}, q_{i,o} \rangle)$ if and only if $(\pi_{i,m}, \pi_{i,n}) \in \to_i$ and $q_{i,p} \in \Delta_i(q_{i,o}, L_i(\pi_{i,m}))$, $Q'_{i,0} := \Pi_{i,0} \times Q_{i,0}$ is the set of initial states, $\mathcal{F}'_i := \Pi_i \times \mathcal{F}_i$ is the set of accepting states, and $W'_i : \Delta'_i \to \mathbb{R}_{\geq 0}$ is the weight function indicating the Euclidean distance for a transition. By following the approach in [14, Section IV] and applying a modified Dijkstra search algorithm [15, Algorithm 3], we find a run in prefix–suffix structure $\tilde{q}_i := q'_{i,j_0} q'_{i,j_1} \cdots = \langle \pi_{i,j_0}, q_{i,j_0} \rangle \langle \pi_{i,j_1}, q_{i,j_1} \rangle \ldots$ with $\tau_i := \pi_{i,j_0} \pi_{i,j_1} \ldots$ so that $(Word(\tau_i), 0) \models \phi_i$. This then implies that agent i has to move from region π_{i,j_k} to region $\pi_{i,j_{k+1}}$ for each $k \geq 0$ by applying the corresponding navigation controller $\boldsymbol{u}_i$ to satisfy ϕ.

B. Signal Temporal Logic

Considering a predicate μ_i associated with an agent $i \in \{M_{\text{LTL}}, +1, \ldots, M\}$, we use the STL fragment of [31] as

$$\psi_i ::= \top \mid \mu_i \mid \neg \mu_i \mid \psi'_i \wedge \psi''_i \tag{3a}$$

$$\phi_i ::= G_{[a_i,b_i]} \psi_i \mid F_{[a_i,b_i]} \psi_i \tag{3b}$$

where ψ'_i and ψ''_i in (3a) are formulas of class ψ_i given in (3a). Note that, unlike LTL operators, $G_{[a_i,b_i]}$ (always) and $F_{[a_i,b_i]}$ (eventually) are time restricted on $[a_i, b_i]$ where $a_i, b_i \in \mathbb{R}_{\geq 0}$ with $a_i \leq b_i$. The satisfaction of μ_i depends on the behavior of agent i and possibly on the behavior of other agents $j \in \mathcal{V} \setminus \{i\}$. If the satisfaction of ϕ_i depends on the behavior of $j \in \mathcal{V}$, i.e., on $\boldsymbol{x}_j(t)$, we say that agent v_j is participating in ϕ_i. The formula ϕ_i consequently depends on a set of agents $\mathcal{V}_i := \{v_{j_1}, \ldots, v_{j_{P_i}}\} \subseteq \mathcal{V}$ where P_i indicates the total number of participating agents. Define $\bar{\boldsymbol{x}}_i(t) := \begin{bmatrix} \boldsymbol{x}_{j_1}(t)^T & \ldots & \boldsymbol{x}_{j_{P_i}}(t)^T \end{bmatrix}^T \in \mathbb{R}^{3P_i}$ and let $\bar{\boldsymbol{x}}_i : \mathbb{R}_{\geq 0} \to \mathbb{R}^{3P_i}$ be the solution to (1). A predicate μ_i is evaluated at time t by its predicate function $h_i : \mathbb{R}^{3P_i} \to \mathbb{R}$ as

$$\mu_i := \begin{cases} \top, & \text{if } h_i(\bar{\boldsymbol{x}}_i(t)) \geq 0 \\ \bot, & \text{if } h_i(\bar{\boldsymbol{x}}_i(t)) < 0. \end{cases}$$

The semantics of STL are given in [19, Definition 1] and stated as a relation $(\bar{\boldsymbol{x}}_i, t) \models \phi_i$, which means that $\bar{\boldsymbol{x}}_i$ satisfies ϕ_i at t. For instance, $(\bar{\boldsymbol{x}}_i, 0) \models \phi_i$ with $\phi_i := G_{[5,10]} \mu'_i \wedge F_{[10,15]} \mu''_i$ implies that $\forall t' \in [5, 10]$, $h'_i(\bar{\boldsymbol{x}}_i(t')) \geq 0$ and $\exists t'' \in [10, 15]$ such that $h''_i(\bar{\boldsymbol{x}}_i(t'')) \geq 0$. Note that μ'_i and μ''_i in the above-mentioned example can encode agent formations, connectivity constraints, or other collaborative tasks that couple agents due to the use of the stacked vector $\bar{\boldsymbol{x}}_i$. STL admits robust semantics [20], while we use a modified version thereof similar to [31] by underapproximating the min-operator of conjunctions in the original semantics as

$$\begin{aligned} \rho^{\mu_i}(\bar{\boldsymbol{x}}_i, t) &:= h_i(\bar{\boldsymbol{x}}_i(t)) \\ \rho^{\neg \mu_i}(\bar{\boldsymbol{x}}_i, t) &:= -h_i(\bar{\boldsymbol{x}}_i(t)) \\ \rho^{\psi'_i \wedge \psi''_i}(\bar{\boldsymbol{x}}_i, t) &:= -\frac{1}{\eta} \ln \Big(\exp \Big(-\eta \rho^{\psi'_i}(\bar{\boldsymbol{x}}_i, t) \Big) \\ &\qquad + \exp \Big(-\eta \rho^{\psi''_i}(\bar{\boldsymbol{x}}_i, t) \Big) \Big) \\ \rho^{G_{[a_i,b_i]} \psi_i}(\bar{\boldsymbol{x}}_i, t) &:= \min_{t_1 \in [t+a_i, t+b_i]} \rho^{\psi_i}(\bar{\boldsymbol{x}}_i, t_1) \\ \rho^{F_{[a_i,b_i]} \psi_i}(\bar{\boldsymbol{x}}_i, t) &:= \max_{t_1 \in [t+a_i, t+b_i]} \rho^{\psi_i}(\bar{\boldsymbol{x}}_i, t_1) \end{aligned}$$

where $\eta > 0$ with the property that $\lim_{\eta \to \infty} \rho^{\psi'_i \wedge \psi''_i}(\bar{\boldsymbol{x}}_i, t) = \min(\rho^{\psi'_i}(\bar{\boldsymbol{x}}_i, t), \rho^{\psi''_i}(\bar{\boldsymbol{x}}_i, t))$; $\rho^{\phi_i}(\bar{\boldsymbol{x}}_i, t)$ states how robustly $\bar{\boldsymbol{x}}_i$ satisfies ϕ_i at time t and we have $(\bar{\boldsymbol{x}}_i, t) \models \phi_i$ if $\rho^{\phi_i}(\bar{\boldsymbol{x}}_i, t) > 0$ [21, Proposition 16]. Formulas of class ψ_i in (3a) are boolean formulas and t is contained in $\rho^{\psi_i}(\bar{\boldsymbol{x}}_i, t)$ through the composition of ρ^{ψ_i} with $\bar{\boldsymbol{x}}_i$ so that we use the shorthand notation $\rho^{\psi_i}(\bar{\boldsymbol{x}}_i(t))$.

Assumption 1: Each ψ_i in (3b) is: 1) s.t. $\rho^{\psi_i}(\bar{\boldsymbol{x}}_i)$ is concave; 2) well posed in the sense that $\rho^{\psi_i}(\bar{\boldsymbol{x}}_i) > 0$ implies $\|\bar{\boldsymbol{x}}_i\| \leq \bar{C}$ for some $\bar{C} \geq 0$; and 3) η is s.t. $\rho^{\psi_i}(\bar{\boldsymbol{x}}_i) > 0$ for some $\bar{\boldsymbol{x}}_i \in \mathbb{R}^{3P_i}$.

Assumption 2: The function $\boldsymbol{w}_i : \mathbb{R}_{\geq 0} \to \mathbb{R}^3$ is piecewise continuous, $f_i : \mathbb{R}^3 \to \mathbb{R}^3$ and $g_i : \mathbb{R}^3 \to \mathbb{R}^{3 \times m_i}$ are locally Lipschitz continuous, and $g_i(\boldsymbol{x}_i) g_i(\boldsymbol{x}_i)^T$ is positive definite.

Remark 1: Part 3 of Assumption 1 implies that ψ_i is satisfiable, i.e., $\exists \bar{\boldsymbol{x}}_i \in \mathbb{R}^{3P_i}$ s.t. $(\bar{\boldsymbol{x}}_i, 0) \models \psi_i$, while Part 2 of Assumption 1 and Assumption 2 guarantee, in conjunction with $\boldsymbol{u}_i$ proposed later, the existence of a solution $\boldsymbol{x}_i(t)$ to (1) defined for all $t \geq 0$. Part 1 of Assumption 1 implies that only concave predicate functions $h_i(\bar{\boldsymbol{x}}_i)$ are allowed which includes the class of linear functions; $g_i(\boldsymbol{x}_i) g_i(\boldsymbol{x}_i)^T$ being positive definite implies that $m_i \geq n_i$, see [31, Remarks 1–3].

The controller in [31] relies on two steps. First, a funnel-based control law is derived when all agents in $\mathcal{V}_i$ are subject to the same task. According to [31, Th. 2], if for all agents $i, j \in \mathcal{V}_i$, we have $\phi_i = \phi_j$ and $(i, j) \in \mathcal{E}$, and all $i \in \mathcal{V}_i$ apply

$$\boldsymbol{u}_{\text{nom},i}(\bar{\boldsymbol{x}}_i, t) := -\epsilon_i(\bar{\boldsymbol{x}}_i, t) g_i(\boldsymbol{x}_i)^T \frac{\partial \rho^{\psi_i}(\bar{\boldsymbol{x}}_i)}{\partial \boldsymbol{x}_i} \tag{4}$$

where $\epsilon_i(\bar{\boldsymbol{x}}_i, t) := \ln(-(\xi_i(\bar{\boldsymbol{x}}_i, t) + 1)/\xi_i(\bar{\boldsymbol{x}}_i, t))$, $\xi_i(\bar{\boldsymbol{x}}_i, t) := (\rho^{\psi_i}(\bar{\boldsymbol{x}}_i) - \rho_i^{\max})/\gamma_i(t)$ with $\rho_i^{\max}$ and $\gamma_i(t)$ as explained in [31, eqs. (6)–(11)] and $\xi_i(\bar{\boldsymbol{x}}_i, t) = \xi_j(\bar{\boldsymbol{x}}_i, t)$ for all $i, j \in \mathcal{V}_i$, then $0 < r_i \leq \rho^{\phi_i}(\bar{\boldsymbol{x}}_i, 0) < \rho_i^{\max}$ so that $(\bar{\boldsymbol{x}}_i, 0) \models \phi_i$, and $r_i > 0$ is a parameter that indicates the robustness by which ϕ_i is satisfied. The idea behind (4) is shown in Fig. 2 (left); (4) confines $\rho^{\psi_i}(\bar{\boldsymbol{x}}_i(t))$ within the funnel given by the red curves and achieves $-\gamma_i(t) + \rho_i^{\max} < \rho^{\psi_i}(\bar{\boldsymbol{x}}_i(t)) < \rho_i^{\max}$ for all $t \geq 0$. By the choice of γ_i, it follows that $r_i \leq \rho^{\phi_i}(\bar{\boldsymbol{x}}_i, 0) < \rho_i^{\max}$. In the second step of [31], dealing with cases where agents in $\mathcal{V}_i$ are subject to different tasks, the conditions in [31, Th. 2] do not hold. If (4) is still applied by each agent i, (4) may become singular since $\epsilon_i(\bar{\boldsymbol{x}}_i(t), t) \to \infty$ as $\rho^{\psi_i}(\bar{\boldsymbol{x}}_i(t)) \to \{-\gamma_i(t) + \rho_i^{\max}, \rho_i^{\max}\}$. We use (4) in conjunction with an online detection and repair scheme that takes care of *critical events*, which are the events where $\rho^{\psi_i}(\bar{\boldsymbol{x}}_i(t)) \in \{-\gamma_i(t) + \rho_i^{\max}, \rho_i^{\max}\}$. Upon detection of a critical event, three repair stages are initiated. The *first repair stage* enlarges the funnel as shown in Fig. 2 (right) by relaxing r_i, $\rho_i^{\max}$, and γ_i (see [31, Section 3.2] for details); r_i remains positive, while γ_i is such that $0 < r_i \leq \rho^{\phi_i}(\bar{\boldsymbol{x}}_i, 0) < \rho_i^{\max}$ if no further critical event occurs. Let N_i indicate the maximum number of critical events in the first repair stage. After detection of N_i critical events in the first stage, the *second repair stage* is enabled if, in case

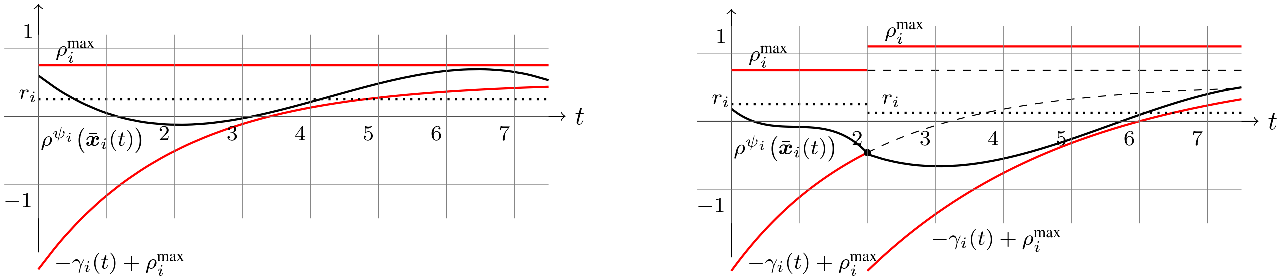

Fig. 2. Funnel-based control law for $G_{[5,7]}\psi_i$ with $r_i := 0.25$ (left). Funnel repairs in the first repair stage (right).

that all agents in $\mathcal{V}_i$ first satisfy ϕ_i collaboratively, there is enough time left so that all agents $j \in \mathcal{V}_i \setminus \{i\}$ can satisfy ϕ_j afterward. The funnel is enlarged the same way as in the first repair stage and all agents $j \in \mathcal{V}_i \setminus \{i\}$ replace, temporarily, $\epsilon_j(\bar{\boldsymbol{x}}_j, t)$, $\rho^{\psi_j}(\bar{\boldsymbol{x}}_j)$, and ψ_j in (4) by $\epsilon_i(\bar{\boldsymbol{x}}_i, t)$, $\rho^{\psi_i}(\bar{\boldsymbol{x}}_i)$, and ψ_i, respectively, to collaboratively satisfy ϕ_i by [31, Th. 2], i.e., the agents $j \in \mathcal{V}_i \setminus \{i\}$ are subject to ϕ_i until ϕ_i is satisfied. If the second repair stage is not enabled, the *third repair stage* is enabled. At each further critical event the funnel is relaxed as in Fig. 2 (right), but now by allowing $r_i < 0$. In particular, we set $r_i = r_i - \delta_i$, where $\delta_i > 0$ is a design parameter. As a consequence, the control law in (4) changes since $\epsilon_i(\bar{\boldsymbol{x}}_i, t)$ and $\rho^{\psi_i}(\bar{\boldsymbol{x}}_i)$ change due to the change in r_i, $\rho_i^{\max}$, and γ_i. By [31, Th. 3], it holds that $\rho^{\phi_i}(\bar{\boldsymbol{x}}_i, 0) \geq \bar{r}_i$ where $\bar{r}_i$ is maximized.

C. Problem Formulation

In the remainder of this brief, we use the term *robot* instead of agent due to the use of mobile robots in the experiments. In particular, we consider a group of mobile robots, where the robots have different sensing and actuation capabilities. Each robot indexed by $i \in \{1, \dots, M_{\text{LTL}}\}$ is subject to an LTL formula ϕ_i of the form (2) and each each robot indexed by $i \in \{M_{\text{LTL}}+1, \dots, M\}$ is subject to an STL formula ϕ_i of the form (3b). The objectives are, based on Sections II-A and II-B, to implement a control algorithm so that:

1) for each $i \in \{1, \dots, M_{\text{LTL}}\}$, $(\sigma_i, 0) \models \phi_i$;
2) for each $i \in \{M_{\text{LTL}}+1, \dots, M\}$, $\rho^{\phi_i}(\bar{\boldsymbol{x}}_i, 0) \geq \bar{r}_i$ where $\bar{r}_i$ is maximized;
3) and, for each $i, j \in \mathcal{V}$ with $i \neq j$, $\|\boldsymbol{x}_i(t) - \boldsymbol{x}_j(t)\| \geq R_{i,j}$ for all $t \geq 0$ where $R_{i,j}$ depends on the agents' geometry, i.e., collisions are mutually avoided.

For the STL approach, we, in particular, need to account for input limitations that are not considered in [31]. Furthermore, we want to show that Assumption 2 is not restrictive in practice when omnidirectional robots are considered. Finally, our goal is to show the computationally efficient and robust nature of our control strategies and that considering LTL and STL mission specifications at the same time can be beneficial.

III. Multi-Robot Systems Under LTL and STL

The implementation of our framework, which can be found in [33], is written in *Python* and *C++* and embedded in the *robot operating system* (ROS) [34]. In the experiments, Turtlebots and Nexus 4WD Mecanum Robotic Cars, which are omnidirectional robots, are considered (see Fig. 1). The omnidirectional robots satisfy Assumption 2, while this is not the case for the Turtlebots. The omnidirectional robots are, hence, subject to STL tasks, while the TurtleBots are subject to LTL tasks. Due to different sensing and actuation capabilities, different communication and control strategies are derived, resulting in different degrees of decentralization.

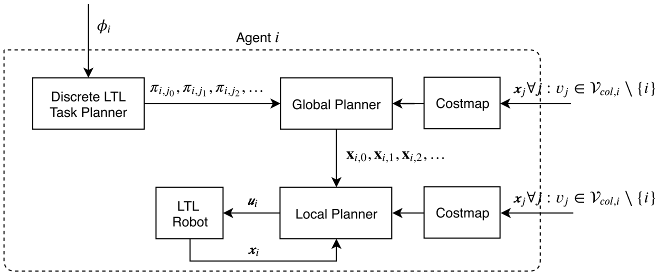
ϕ_i
Agent i
Discrete LTL Task Planner
$\pi_{i,j_0}, \pi_{i,j_1}, \pi_{i,j_2}, \dots$
Global Planner
Costmap
$\boldsymbol{x}_j \forall j : v_j \in \mathcal{V}_{col,i} \setminus \{i\}$
$\mathbf{x}_{i,0}, \mathbf{x}_{i,1}, \mathbf{x}_{i,2}, \dots$
LTL Robot
$\boldsymbol{u}_i$
Local Planner
Costmap
$\boldsymbol{x}_j \forall j : v_j \in \mathcal{V}_{col,i} \setminus \{i\}$
$\boldsymbol{x}_i$

Fig. 3. Control architecture used for robots under LTL tasks.

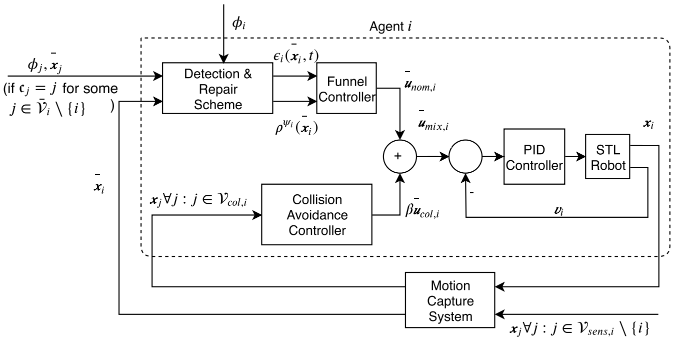
ϕ_i
Agent i
$\phi_j, \bar{\boldsymbol{x}}_j$
(if $\mathfrak{c}_j = j$ for some $j \in \bar{\mathcal{V}}_i \setminus \{i\}$)
Detection & Repair Scheme
$\epsilon_i(\bar{\boldsymbol{x}}_i, t)$
$\rho^{\psi_i}(\bar{\boldsymbol{x}}_i)$
Funnel Controller
$\bar{\boldsymbol{u}}_{nom,i}$
$\bar{\boldsymbol{u}}_{mix,i}$
+
PID Controller
STL Robot
$\boldsymbol{x}_i$
$\bar{\boldsymbol{x}}_i$
$\boldsymbol{x}_j \forall j : j \in \mathcal{V}_{col,i}$
Collision Avoidance Controller
$\beta\bar{\boldsymbol{u}}_{col,i}$
-
v_i
Motion Capture System
$\boldsymbol{x}_j \forall j : j \in \mathcal{V}_{sens,i} \setminus \{i\}$

Fig. 4. Control architecture used for robots under STL tasks.

A. LTL Tasks

TurtleBots are modeled with $f_i(\boldsymbol{x}_i) := \mathbf{0}_3$ and $g_i(\boldsymbol{x}_i) := [\cos(x_{i,3})u_{i,1} \;\; \sin(x_{i,3})u_{i,1} \;\; u_{i,2}]^T$ in (1). Sensing is performed locally by the use of onboard sensors with a directional field of view. Let $\mathcal{V}_{\text{col},i}(t) \subseteq \mathcal{V} \setminus \{i\}$ denote the set of agents that are in the field of view at time t, to be used for collision avoidance. Since LTL tasks are not coupled (as assumed in Section II-A) and due to local sensing, no communication between robots in $i \in \{1, \dots, M_{\text{LTL}}\}$ is needed. The control architecture is shown in Fig. 3. The discrete LTL task planner, introduced in Section II-A, is further summarized in Algorithm 1 below.

Navigation according to the obtained high-level LTL plan τ_i while adhering to collision avoidance is achieved by the

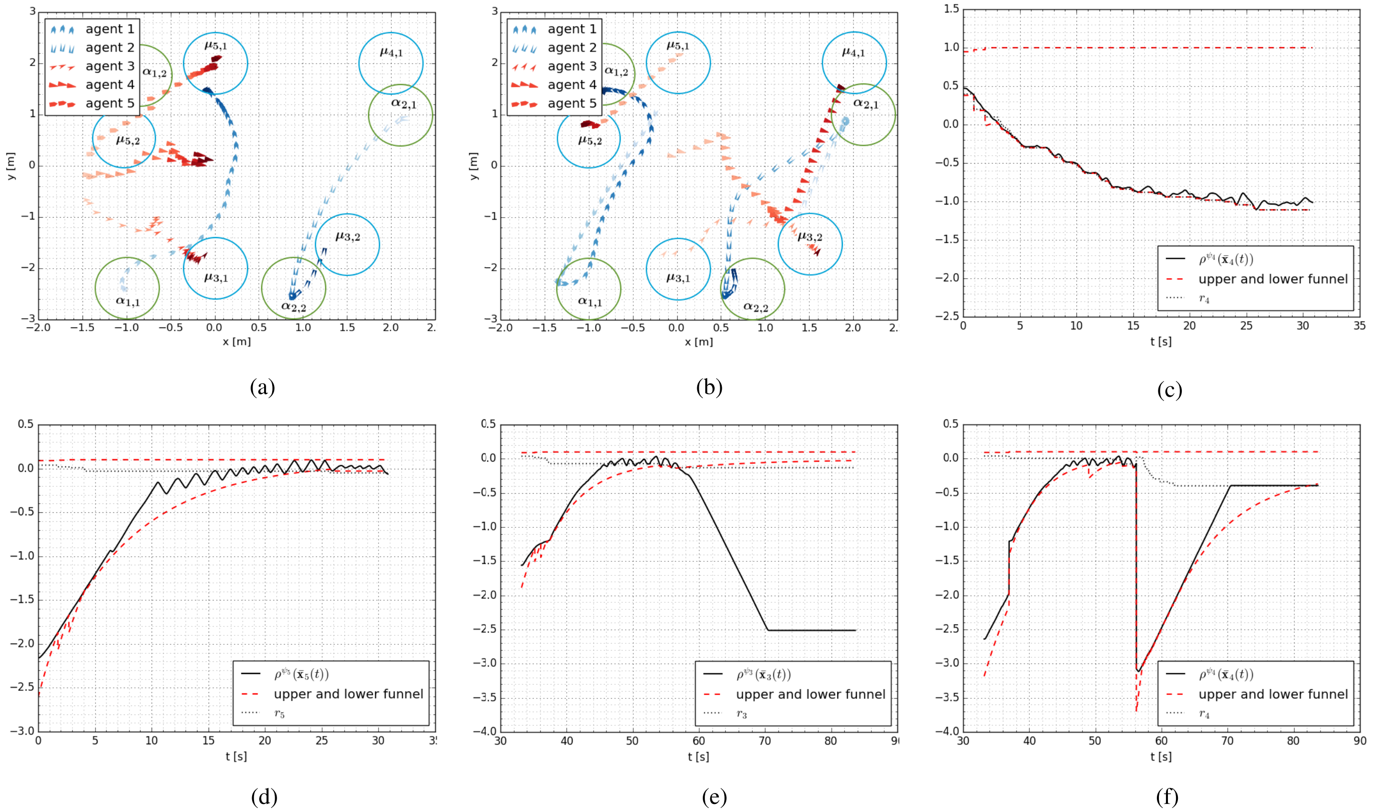

(a) (b) (c)

(d) (e) (f)

Fig. 5. Robot trajectories and evolution of the robust semantics for selected robots of Scenario 1. (a) Robot trajectories from 0 to 30 s. (b) Robot trajectories from 30 to 90 s. (c) Robust semantics $\rho^{\psi'_4}(\bar{x}_4(t))$ for ϕ'_4. (d) Robust semantics $\rho^{\psi'_5}(\bar{x}_5(t))$ for ϕ'_5. (e) Robust semantics $\rho^{\psi''_3}(\bar{x}_3(t))$ for ϕ''_3. (f) Robust semantics $\rho^{\psi''_4}(\bar{x}_4(t))$ for ϕ''_4.

Algorithm 1 Discrete LTL Task Planner for Robot i

```
Form $\mathcal{A}_{\phi_i}$ corresponding to $\phi_i$
Construct $\mathcal{T}_i$ considering the poses of interest in $\Pi_i$
Construct the product automaton $\mathcal{A}'_{\phi_i} := \mathcal{T}_i \times \mathcal{A}_{\phi_i}$
Apply the modified Dijkstra search algorithm [15, Alg. 3]
    to obtain $\tilde{q}_i := q'_{i,j_0} q'_{i,j_1} \cdots = \langle \pi_{i,j_0}, q_{i,j_0} \rangle \langle \pi_{i,j_1}, q_{i,j_1} \rangle \ldots$
Output $\tau_i := \pi_{i,j_0} \pi_{i,j_1} \ldots$
```

combination of a global (ROS package *global_planner*) and a local (ROS package *dwa_local_planner*) planner within the *move_base* ROS package. The global planner finds, using a Dijkstra algorithm, a set of sampled waypoints $\mathbf{x}_{i,0}$, $\mathbf{x}_{i,1}$, $\mathbf{x}_{i,2}$, $\ldots$ which sequentially connect the initial position $\boldsymbol{x}_i(0)$ and the poses of interest π_{i,j_0}, π_{i,j_1}, π_{i,j_2}, $\ldots$ as closely as possible while taking into account obstacles that may result in a collision. The set of waypoints is then followed in the local planner as accurately as possible by avoiding these obstacles under consideration of the robot dynamics in (1) using the dynamic window approach [35], outputting $\boldsymbol{u}_i(t)$. Both global and local planner take obstacles into account by creating a dynamic cost map using the ROS package *costmap_2d*, which is based on the local sensors of each turtlebot. This package creates a grid of the workspace with different costs for each cell in the grid, indicating how close the robot is in the vicinity to an obstacle and how close the robot is to the goal. Local and global cost maps are different since the goals for the global planner are poses of interest π_{i,j_0}, π_{i,j_1}, π_{i,j_2}, $\ldots$, while the local planner considers the waypoints $\mathbf{x}_{i,0}$, $\mathbf{x}_{i,1}$, $\mathbf{x}_{i,2}$, $\ldots$.

B. STL Tasks

Using the approach presented in Section II-B, we assume the dynamics in (1) with unkown $f_i(\boldsymbol{x}_i)$. For the omnidirectional robots, it holds that $m_i := 3$. Since $g_i(\boldsymbol{x}_i)$ is a square matrix, it is straightforward to show that

$$\boldsymbol{u}_{\text{nom},i}(\bar{\boldsymbol{x}}_i, t) := -\epsilon_i(\bar{\boldsymbol{x}}_i, t)\frac{\partial \rho^{\psi_i}(\bar{\boldsymbol{x}}_i)}{\partial \boldsymbol{x}_i} \tag{5}$$

gives the same guarantees as (4), but without knowing $f_i(\boldsymbol{x}_i)$ and $g_i(\boldsymbol{x}_i)$ illustrating the robustness of the controller. Hence, $\boldsymbol{u}_{\text{nom},i}(\bar{\boldsymbol{x}}_i, t)$ as in (5) will be used instead of (4). The control architecture is shown in Fig. 4. For collision avoidance, we again only consider robots within a neighborhood of robot i and within a range of R, where $R > R_{i,j}$ for all $j \in \mathcal{V}$, as $\mathcal{V}_{\text{col},i}(t) := \{j \in \mathcal{V} | \|\boldsymbol{x}_i(t) - \boldsymbol{x}_j(t)\| \leq R\}$. Sensing is done by means of a motion capture system that can be replaced, in experiments performed outside the laboratory, by using laser range finders [36] or visual odometry [37]. Let us define $\mathcal{V}_{\text{sens},i}(t) := \mathcal{V}_i \cup \mathcal{V}_{\text{col},i}(t)$ to denote the robot information that is needed at time t. In [31], we have shown that the control law $\beta_i \boldsymbol{u}_{\text{col},i}(\boldsymbol{x}) + \boldsymbol{u}_{\text{nom},i}(\bar{\boldsymbol{x}}_i, t)$ with $\beta_i \geq 0$ provides the same guarantees as [31, Th. 2] when $\boldsymbol{u}_{\text{col},i}(\boldsymbol{x})$, used for collision avoidance, is locally Lipschitz continuous in $\boldsymbol{x}$. In real physical

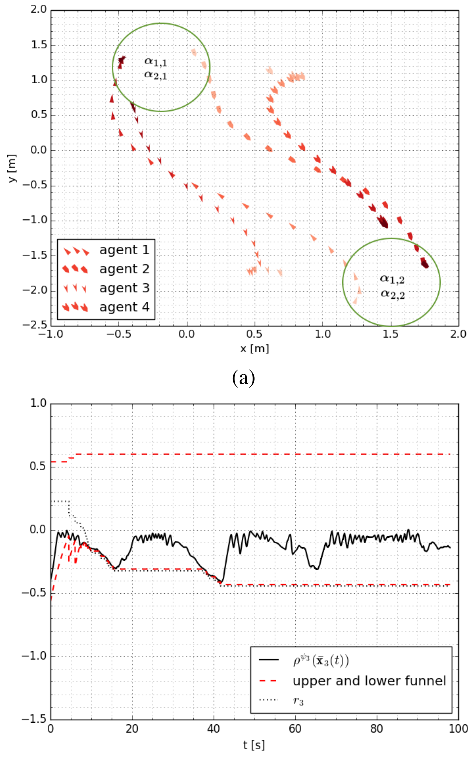

(a)

(b)

Fig. 6. Robot trajectories and robust semantics for Scenario 2. (a) Robot trajectories from 23 to 45 s. (b) Robust semantics $\rho^{\psi_3}(\bar{\boldsymbol{x}}_3(t))$ for ϕ_3.

systems, however, the input is limited by $u_{\max,i} \in \mathbb{R}_{\geq 0}$, and hence, we first define

$$\bar{\boldsymbol{u}}_{\text{nom},i}(\bar{\boldsymbol{x}}_i,t) := \begin{cases} \boldsymbol{u}_{\text{nom},i}(\bar{\boldsymbol{x}}_i,t), & \text{if } \|\boldsymbol{u}_{\text{nom},i}(\bar{\boldsymbol{x}}_i,t)\| \leq u_{\max,i} \\ u_{\max,i}\dfrac{\boldsymbol{u}_{\text{nom},i}(\bar{\boldsymbol{x}}_i,t)}{\|\boldsymbol{u}_{\text{nom},i}(\bar{\boldsymbol{x}}_i,t)\|}, & \text{otherwise} \end{cases}$$

and $\bar{\boldsymbol{u}}_{\text{col},i}(\boldsymbol{x}) := [\tilde{\boldsymbol{u}}_{\text{col},i}(\boldsymbol{x})^T \;\; 0]^T$ where, for $R_1 < R$

$$\tilde{\boldsymbol{u}}_{\text{col},i}(\boldsymbol{x}) := \sum_{j\in\mathcal{V}:\|z_i-z_j\|<R_1} u_{\max,i} D(z_i,z_j) + \sum_{j\in\mathcal{V}:R_1\leq\|z_i-z_j\|\leq R} k_i \left(\frac{R-\|z_i-z_j\|}{\|z_i-z_j\|^3 R}\right) D(z_i,z_j)$$

with $D(z_i,z_j) := (z_i - z_j)/\|z_i - z_j\|$ and where $k_i := u_{\max,i} R R_1^3/(R - R_1)$ ensures that $\bar{\boldsymbol{u}}_{\text{col},i}(\boldsymbol{x})$ is continuous. Let $\boldsymbol{u}_{\text{mix},i}(\boldsymbol{x},t) := \beta_i \bar{\boldsymbol{u}}_{\text{col},i}(\boldsymbol{x}) + \bar{\boldsymbol{u}}_{\text{nom},i}(\bar{\boldsymbol{x}}_i,t)$ so that we define the control law

$$\bar{\boldsymbol{u}}_{\text{mix},i}(\boldsymbol{x},t) := \begin{cases} \boldsymbol{u}_{\text{mix},i}(\boldsymbol{x},t), & \text{if } \|\boldsymbol{u}_{\text{mix},i}(\boldsymbol{x},t)\| \leq u_{\max,i} \\ u_{\max,i}\dfrac{\boldsymbol{u}_{\text{mix},i}(\boldsymbol{x},t)}{\|\boldsymbol{u}_{\text{mix},i}(\boldsymbol{x},t)\|}, & \text{otherwise.} \end{cases} \tag{6}$$

The parameter β_i determines how much collision avoidance is taken into account. For only two robots, $\beta_i \geq 1$ ensures collision avoidance since $\bar{\boldsymbol{u}}_{\text{col},i}(\boldsymbol{x})$ dominates $\bar{\boldsymbol{u}}_{\text{nom},i}(\bar{\boldsymbol{x}}_i,t)$. The obtained control commands (6) are forwarded to a low-level PID controller that is integrated into each omnidirectional robot to track these velocity commands. Input limitations, the collision avoidance mechanism, and the digital implementation of (6) are the reason why the guarantees of [31, Th. 2] do not hold anymore. As a result, more critical events may occur. As shown in Section IV, satisfactory behavior can still be achieved when deadlines of the STL task are not too tight due to the detection and repair scheme, as summarized in Algorithm 2.

Algorithm 2 Detection and Repair Scheme for Robot i

```
1:  Calculate initial $r_i$, $\rho_i^{\max}$, $\gamma_i$ [31, Sec. 3.2]
2:  Set $ce := 0$                              ▷ Counter for critical events
3:  Set $\mathfrak{c}_i := 0$                   ▷ Indicates 2nd repair stage
4:  repeat
5:      if Critical Event and $\mathfrak{c}_j := 0$ for all $i \in \mathcal{V}_j \setminus \{j\}$ then
6:          Set $ce := ce + 1$
7:          if $ce \leq N_i$ then                ▷ 1st repair stage
8:              Calculate new $r_i$, $\rho_i^{\max}$, $\gamma_i$ [31, Sec. 3.2]
9:          else                                 ▷ 2nd and 3rd repair stages
10:             if 2nd repair stage and $\mathfrak{c}_i = 0$ then
11:                 Calculate new $r_i$, $\rho_i^{\max}$, $\gamma_i$ [31, Sec. 3.2]
12:                 Set $\mathfrak{c}_i := i$; send $\rho_i^{\max}$, $\gamma_i$, $\psi_i$ to $j \in \mathcal{V}_i \setminus \{i\}$
13:             else if 2nd repair stage and $\mathfrak{c}_i = i$ then
14:                 $r_i := r_i - \delta_i$; Calculate new $\rho_i^{\max}$, $\gamma_i$
15:                 Send $\rho_i^{\max}$, $\gamma_i$, $\psi_i$ to $j \in \mathcal{V}_i \setminus \{i\}$
16:             else 3rd repair stage
17:                 $r_i := r_i - \delta_i$; Calculate new $\rho_i^{\max}$, $\gamma_i$
18:             end if
19:         end if
20:         if $\mathfrak{c}_j = j$ and $i \in \mathcal{V}_j \setminus \{j\}$ then▷ 2nd repair stage
21:             Set $\rho_i^{\max} := \rho_j^{\max}$, $\gamma_i := \gamma_j$, $\psi_i := \psi_j$
22:         end if
23:         if $\mathfrak{c}_j$ changed from $j$ to $-1$ and $i \in \mathcal{V}_j \setminus \{j\}$ then
24:             Reset $\psi_i$, Calculate new $r_i$, $\rho_i^{\max}$, $\gamma_i$
25:         end if
26:     end if
27:     Calculate and output $\epsilon(\bar{\boldsymbol{x}}_i, t)$ and $\rho^{\psi_i}(\bar{\boldsymbol{x}}_i)$
28: until $\rho^{\phi_i}(\bar{\boldsymbol{x}}_i, 0) \geq \bar{r}_i$ where $\bar{r}_i$ is maximized.
29: Set $\mathfrak{c}_i := -1$
```

Algorithm 2 follows Section II-B and uses a parameter $\mathfrak{c}_i$ indicating, when $\mathfrak{c}_i \notin \{0, -1\}$, that the second repair stage has been initiated by agent i (lines 10–12). Agents $j \in \mathcal{V}_i \setminus \{i\}$ then collaborate to satisfy ϕ_i (lines 20–21). If ϕ_i is satisfied, collaboration is terminated and $\mathfrak{c}_i = -1$ (line 29) so that robots in $j \in \mathcal{V}_i \setminus \{i\}$ can continue with ϕ_j (line 24). We obtain $\rho^{\phi_i}(\bar{\boldsymbol{x}}_i, 0) \geq \bar{r}_i$, where $\bar{r}_i$ is maximized (line 28).

IV. Experimental Results

We now present the experimental results for three different scenarios that were performed on a rectangular workspace of size $[-3.5, -3.5] \times [3.5, 3.5]$ (measured in meters). Videos of the three scenarios can be found in [38]–[40], respectively.

Scenario 1: The first scenario demonstrates the full functionality of the presented framework. We employ $M_{\text{LTL}} = 2$ and $M_{\text{STL}} = 3$ robots. For robots 1 and 2, we define the propositions $\alpha_{1,1}$, $\alpha_{1,2}$, $\alpha_{2,1}$, and $\alpha_{2,2}$, as shown in Fig. 5. The LTL tasks are $\phi_1 := GF(\alpha_{1,1} \wedge \alpha_{1,2})$ and $\phi_2 := GF(\alpha_{2,1} \wedge \alpha_{2,2})$

or, in words, robot 1 (robot 2) should periodically visit $\alpha_{1,1}$ and $\alpha_{1,2}$ ($\alpha_{2,1}$ and $\alpha_{2,2}$). For robot 3, define $\mu_{3,1} := (\|z_3 - [0 \;\; -2]^T\| \leq 0.1)$, $\mu_{3,2} := (\|z_3 - [1.5 \;\; -1.5]^T\| \leq 0.1)$, $\mu_{3,3} := (\|z_3 - z_4\| \leq 0.7)$, $\phi_3' := G_{[21,30]}\mu_{3,1}$, and $\phi_3'' := F_{[57,58]}(\mu_{3,2} \wedge \mu_{3,3})$. Robot 3 is then subject to $\phi_3 := \phi_3' \wedge \phi_3''$ or, in words, always between 21 and 30 s be in region $\mu_{3,1}$ and eventually between 57 and 58 s be in region $\mu_{3,2}$ while being at least 0.7 m close to robot 4. For robot 4, define $\mu_{4,1} := (\|z_4 - [2 \;\; 2]^T\| \leq 0.1)$, $\mu_{4,2} := (\|z_4 - z_3\| \leq 1)$, $\mu_{4,3} := (\|z_4 - z_5\| \leq 1)$, $\phi_4' := G_{[5,30]}(\mu_{4,2} \wedge \mu_{4,3})$, and $\phi_4'' := F_{[83,87]}\mu_{4,1}$. Robot 4 is subject to $\phi_4 := \phi_4' \wedge \phi_4''$ or, in words, always between 5 and 30 s be 1 m close to agents 3 and 5 and eventually between 83 and 87 s be in region $\mu_{4,1}$. Robot 5 should always between 21 and 30 s be in region $\mu_{5,1}$ and eventually between 44 and 47 s be in region $\mu_{5,2}$. where $\mu_{5,1} := (\|z_5 - [0 \;\; 2]^T\| \leq 0.1)$ and $\mu_{5,2} := (\|z_5 - [-1 \;\; 0.5]^T\| \leq 0.1)$ so that $\phi_5 := \phi_5' \wedge \phi_5''$ where $\phi_5' := G_{[21,30]}\mu_{5,1}$ and $\phi_5'' := F_{[44,47]}\mu_{5,2}$. The trajectories of the robots for 0-30 seconds and 30-90 seconds are shown in Fig. 5(a) and (b), respectively. The evolution of a robot over time is indicated by increasing color intensity and it can, hence, be seen that collisions are avoided. Note that robots 3 and 4 are coupled to other robots. In Fig. 5(a), showing ϕ_3', ϕ_4', and ϕ_5', robot 4 needs to stay close to robots 3 and 5, while robots 3 and 5 are supposed to move to $\mu_{3,1}$ and $\mu_{5,1}$, respectively, so that agent 4 cannot satisfy ϕ_4'. Robot 4 finds a least violating solution by successively reducing the robustness r_4 [third repair stage, see Fig. 5(c)] and consequently staying as close as possible to robots 3 and 5. Robots 3 and 5 satisfy their tasks ϕ_3' and ϕ_5', respectively, as illustrated for robot 5 in Fig. 5(d). More formally, we have $\rho^{\phi_3'}(\bar{\boldsymbol{x}}_3, 0) \geq -0.18$, $\rho^{\phi_4'}(\bar{\boldsymbol{x}}_4, 0) \geq -1.11$, and $\rho^{\phi_5'}(\bar{\boldsymbol{x}}_5, 0) \geq -0.12$. In Fig. 5(b), showing ϕ_3'', ϕ_4'', and ϕ_5'', robot 3 needs to move to $\mu_{3,2}$ while staying close to robot 4. Robot 4, however, is supposed to move to $\mu_{4,1}$. Therefore, at some point, robot 3 establishes communication with robot 4 to collaboratively satisfy ϕ_3'' [second repair stage, see Fig. 5(e)]. Afterward, robot 4 continues with ϕ_4'' [see Fig. 5(f)]. It holds that $\rho^{\phi_3''}(\bar{\boldsymbol{x}}_3, 0) \geq 0.02$, $\rho^{\phi_4''}(\bar{\boldsymbol{x}}_4, 0) \geq -0.4$, and $\rho^{\phi_5''}(\bar{\boldsymbol{x}}_5, 0) \geq 0.5$. This scenario illustrates how the online detection and repair scheme handles critical events so that, even when obstacles need to be avoided or when local tasks are not satisfiable, $\rho^{\phi_i}(\bar{\boldsymbol{x}}_i, 0) \geq \bar{r}_i$ is achieved, where $\bar{r}_i$ is maximized. As can be seen in the video in [38], the workspace is densely filled with robots so that collision avoidance is the main reason why the robustness $\bar{r}_i$ is decreased.

Scenario 2: In this scenario, we couple robots under STL tasks to robots under LTL tasks to induce periodic motion. Consider $M_{\text{LTL}} = 2$ and $M_{\text{STL}} = 2$ robots. For robots 1 and 2, $\phi_1 := GF(\alpha_{1,1} \wedge \alpha_{1,2})$ and $\phi_2 := GF(\alpha_{2,1} \wedge \alpha_{2,2})$ again encode to periodically visit the regions $\alpha_{1,1}$, $\alpha_{1,2}$ and $\alpha_{2,1}$, $\alpha_{2,2}$, respectively [see Fig. 6(a)]. For robots 3 and 4, define $\mu_3 := (\|z_3 - z_1\| \leq 0.6)$, $\mu_4 := (\|z_4 - z_2\| \leq 0.6)$, $\phi_3 := G_{[0,90]}\mu_3$, and $\phi_4 := G_{[0,90]}\mu_4$, i.e., robots 3 and 4 track robots 1 and 2, respectively. The robots under STL tasks congest the path so that collision are expected. The trajectories of the robots from 23 to 45 s are shown in Fig. 6(a). The LTL tasks ϕ_1 and ϕ_2 are satisfied while the robots under STL tasks track the robots under LTL tasks closely [see Fig. 6(b)]; ϕ_3 and ϕ_4 are not satisfied due to collision avoidance and the induced repair stages; however, we obtain $\rho^{\phi_3}(\bar{\boldsymbol{x}}_3, 0) \geq -0.45$ and $\rho^{\phi_4}(\bar{\boldsymbol{x}}_4, 0) \geq -0.47$.

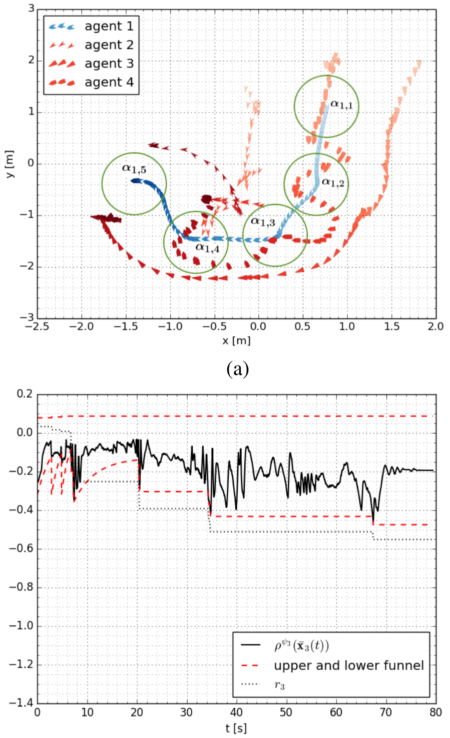

(a)

(b)

Fig. 7. Robot trajectories and robust semantics for Scenario 3. (a) Robot trajectories. (b) Robust semantics $\rho^{\psi_3}(\bar{\boldsymbol{x}}_3(t))$ for ϕ_3.

Scenario 3: We again couple robots to other robots, but in a more complex way. Consider $M_{\text{LTL}} = 1$ and $M_{\text{STL}} = 3$ robots. We have $\phi_1 := F(\alpha_{1,1} \wedge \alpha_{1,2} \wedge \alpha_{1,3} \wedge \alpha_{1,4} \wedge \alpha_{1,5})$ where the propositions can be seen in Fig. 7(a). The method proposed in Section III will find the shortest path satisfying ϕ_1, which is to sequentially move to $\alpha_{1,1}$, $\alpha_{1,2}$, $\alpha_{1,3}$, $\alpha_{1,4}$, and $\alpha_{1,5}$. The robots under STL tasks are supposed to form a formation with respect to the LTL robot and to also track its orientation. Let $\mu_{2,1} := (\|z_2 - z_1 - [\sin(x_{1,3}) \;\; -\cos(x_{1,3})]^T) \leq 0.1$ and $\mu_{2,2} := (|x_{2,3} - x_{1,3}|) \leq 0.09$ so that $\phi_2 := G_{[10,100]}(\mu_{2,1} \wedge \mu_{2,2})$ which means, in words, that robot 2 should always be to the right of robot 1 and track its orientation. Let also $\mu_{3,1} := (\|z_3 - z_1 - [-\sin(x_{1,3}) \;\; \cos(x_{1,3})]^T) \leq 0.1$ and $\mu_{3,2} := (|x_{3,3} - x_{1,3}|) \leq 0.09$ so that $\phi_3 := G_{[10,100]}(\mu_{3,1} \wedge \mu_{3,2})$, i.e., robot 3 should always be to the left of robot 1 and track its orientation. Similarly, ϕ_4, omitted here, means that robot 4 should always be behind robot 1 and track its orientation. The robustness function for robot 3 is shown in Fig. 7(b).

It has been shown that the proposed method is robust in the sense that STL tasks can be satisfied with given robustness. Input limitations, collision avoidance, the digital implementation of (6), or cases not covered by [31, Th. 2], however, may induce critical events that are handled by the detection and repair scheme. The computation times of Algorithm 1 are, on average, 0.5 s. The control loops for robots under LTL and STL tasks are run with 5 and 100 Hz, respectively.

V. Conclusion

We presented the implementation and experimental results of [14] and [31], which present theoretical frameworks for the control of multi-agent systems under LTL and STL tasks. In particular, each agent is represented by a mobile robot that is either subject to a local LTL or a local STL task. Our implementation deals with practical issues, such as collision avoidance, input saturations, the digital implementation of continuous-time feedback control laws, and a controllability assumption that was made in the original works. We also argued that using LTL and STL at the same time can be beneficial. A particular strength of combining these temporal logics is that STL tasks can depend on the agents under periodic LTL tasks. We provided three experiments and have shown that our method can be used as a multipurpose tool. For the future, we plan to introduce a robustness recovery mechanism that can be integrated into the online detection and repair scheme of the STL framework. Thereby, the robustness, by which an STL task is satisfied, can again be increased after the occasion of unforeseen events that potentially decreased this robustness.

References

[1] W. Ren and R. W. Beard, "Consensus seeking in multiagent systems under dynamically changing interaction topologies," *IEEE Trans. Autom. Control*, vol. 50, no. 5, pp. 655–661, May 2005.

[2] H. G. Tanner, A. Jadbabaie, and G. J. Pappas, "Stable flocking of mobile agents, Part I: Fixed topology," in *Proc. 42nd IEEE Int. Conf. Decis. Control*, Maui, HI, USA, Dec. 2003, pp. 2010–2015.

[3] M. M. Zavlanos and G. J. Pappas, "Distributed connectivity control of mobile networks," *IEEE Trans. Robot.*, vol. 24, no. 6, pp. 1416–1428, Dec. 2008.

[4] D. V. Dimarogonas, S. G. Loizou, K. J. Kyriakopoulos, and M. M. Zavlanos, "A feedback stabilization and collision avoidance scheme for multiple independent non-point agents," *Automatica*, vol. 42, no. 2, pp. 229–243, Feb. 2006.

[5] M. Mesbahi and M. Egerstedt, *Graph Theoretic Methods in Multiagent Networks*, 1st ed. Princeton, NY, USA: Princeton Univ. Press, 2010.

[6] C. Baier and J.-P. Katoen, *Principles of Model Checking*, 1st ed. Cambridge, MA, USA: MIT Press, 2008.

[7] M. Kloetzer and C. Belta, "A fully automated framework for control of linear systems from temporal logic specifications," *IEEE Trans. Autom. Control*, vol. 53, no. 1, pp. 287–297, Feb. 2008.

[8] G. E. Fainekos, H. Kress-Gazit, and G. J. Pappas, "Temporal logic motion planning for mobile robots," in *Proc. IEEE Int. Conf. Robot. Automat.*, Barcelona, Spain, Apr. 2005, pp. 2020–2025.

[9] N. Piterman, A. Pnueli, and Y. Sa'ar, "Synthesis of reactive (1) designs," in *Proc. Int. Workshop VMCAI*, Charleston, SC, USA, 2006, pp. 364–380.

[10] H. Kress-Gazit, G. E. Fainekos, and G. J. Pappas, "Temporal-logic-based reactive mission and motion planning," *IEEE Trans. Robot.*, vol. 25, no. 6, pp. 1370–1381, Dec. 2009.

[11] D. Maity and J. S. Baras, "Event-triggered controller synthesis for dynamical systems with temporal logic constraints," in *Proc. Annu. Amer. Control Conf.*, Milwaukee, WI, USA, Jun. 2018, pp. 1184–1189.

[12] T. Wongpiromsarn, U. Topcu, and R. M. Murray, "Receding horizon control for temporal logic specifications," in *Proc. 13th ACM Int. Conf. Hybrid Syst., Comput. Control*, New York, NY, USA, Apr. 2010, pp. 101–110.

[13] S. G. Loizou and K. J. Kyriakopoulos, "Automatic synthesis of multi-agent motion tasks based on LTL specifications," in *Proc. 43rd IEEE Conf. Decis. Control*, vol. 1, Nassau, Bahamas, Dec. 2004, pp. 153–158.

[14] M. Guo, J. Tumova, and D. V. Dimarogonas, "Communication-free multi-agent control under local temporal tasks and relative-distance constraints," *IEEE Trans. Autom. Control*, vol. 61, no. 12, pp. 3948–3962, Dec. 2016.

[15] M. Guo and D. V. Dimarogonas, "Multi-agent plan reconfiguration under local LTL specifications," *Int. J. Robot. Res.*, vol. 34, no. 2, pp. 218–235, 2015.

[16] M. Kloetzer and C. Belta, "Automatic deployment of distributed teams of robots from temporal logic motion specifications," *IEEE Trans. Robot.*, vol. 26, no. 1, pp. 48–61, Feb. 2010.

[17] J. Tumova and D. V. Dimarogonas, "Multi-agent planning under local LTL specifications and event-based synchronization," *Automatica*, vol. 70, pp. 239–248, Aug. 2016.

[18] Y. E. Sahin, P. Nilsson, and N. Ozay, "Synchronous and asynchronous multi-agent coordination with cLTL+ constraints," in *Proc. IEEE 56th Annu. Conf. Decis. Control*. Melbourne, VIC, Australia: IEEE, Dec. 2017, pp. 335–342.

[19] O. Maler and D. Nickovic, "Monitoring temporal properties of continuous signals," in *Proc. FORMATS-FTRTFT*, Grenoble, France, Sep. 2004, pp. 152–166.

[20] A. Donzé and O. Maler, "Robust satisfaction of temporal logic over real-valued signals," in *Proc. Int. Conf. FORMATS*, Klosterneuburg, Austria, Sep. 2010, pp. 92–106.

[21] G. E. Fainekos and G. J. Pappas, "Robustness of temporal logic specifications for continuous-time signals," *Theor. Comput. Sci.*, vol. 410, no. 42, pp. 4262–4291, 2009.

[22] V. Raman, A. Donzé, M. Maasoumy, R. M. Murray, A. Sangiovanni-Vincentelli, and S. A. Seshia, "Model predictive control with signal temporal logic specifications," in *Proc. 53rd IEEE Conf. Decis. Control*, Los Angeles, CA, USA, Dec. 2014, pp. 81–87.

[23] S. Sadraddini and C. Belta, "Robust temporal logic model predictive control," in *Proc. 53rd Annu. Allerton Conf. Commun., Control, Comput.*, Monticello, IL, USA, Sep. 2015, pp. 772–779.

[24] L. Lindemann and D. V. Dimarogonas, "Robust control for signal temporal logic specifications using discrete average space robustness," *Automatica*, vol. 101, pp. 377–387, Mar. 2019.

[25] L. Lindemann and D. V. Dimarogonas, "Control barrier functions for signal temporal logic tasks," *IEEE Control Syst. Lett.*, vol. 3, no. 1, pp. 96–101, Jan. 2019.

[26] S. S. Farahani, R. Majumdar, V. S. Prabhu, and S. E. Z. Soudjani, "Shrinking horizon model predictive control with chance-constrained signal temporal logic specifications," in *Proc. Amer. Control Conf.*, Seattle, WA, USA, May 2017, pp. 1740–1746.

[27] D. Sadigh and A. Kapoor, "Safe control under uncertainty with probabilistic signal temporal logic," in *Proc. Robot. Sci. Syst.*, Ann Arbor, MI, USA, Jun. 2016. [Online]. Available: http://rss2016.engin.umich.edu

[28] S. Sadraddini and C. Belta, "Formal guarantees in data-driven model identification and control synthesis," in *Proc. 21st Int. Conf. Hybrid Syst., Comput. Control*, Porto, Portugal, Apr. 2018, pp. 147–156.

[29] Y. V. Pant, H. Abbas, R. A. Quaye, and R. Mangharam, "Fly-by-logic: Control of multi-drone fleets with temporal logic objectives," in *Proc. 9th ACM/IEEE Int. Conf. Cyber-Phys. Syst.*, Porto, Portugal, Apr. 2018, pp. 186–197.

[30] N. Mehdipour, C.-I. Vasile, and C. Belta, "Arithmetic-geometric mean robustness for control from signal temporal logic specifications," in *Proc. Amer. Control Conf.*, Philadelphia, PA, USA, Jul. 2019, pp. 1690–1695.

[31] L. Lindemann and D. V. Dimarogonas, "Feedback control strategies for multi-agent systems under a fragment of signal temporal logic tasks," *Automatica*, vol. 106, pp. 284–293, Aug. 2019.

[32] Z. Liu, B. Wu, J. Dai, and H. Lin, "Distributed communication-aware motion planning for multi-agent systems from stl and spatel specifications," in *Proc. IEEE 56th Annu. Conf. Decis. Control*, Melbourne, Australia, Dec. 2017, pp. 4452–4457.

[33] *GitHub Code Repository*. Accessed: Feb. 2019. [Online]. Available: https://github.com/KTH-SML/CodeRepositoryTCST

[34] M. Quigley *et al.*, "Ros: An open-source robot operating system," in *Proc. ICRA Workshop Open Source Softw.*, Kobe, Japan, May 2009, vol. 3, nos. 2–3, p. 5.

[35] D. Fox, W. Burgard, and S. Thrun, "The dynamic window approach to collision avoidance," *IEEE Robot. Autom. Mag.*, vol. 4, no. 1, pp. 23–33, Mar. 1997.

[36] H. Surmann, A. Nüchter, and J. Hertzberg, "An autonomous mobile robot with a 3D laser range finder for 3D exploration and digitalization of indoor environments," *Robot. Auton. Syst.*, vol. 45, nos. 3–4, pp. 181–198, 2003.

[37] D. Nister, O. Naroditsky, and J. Bergen, "Visual odometry," in *Proc. IEEE Comput. Soc. Conf. Comput. Vis. Pattern Recognit.*, vol. 1, Washington, DC, USA, Jun./Jul. 2004, p. I.

[38] *Video of Scenario 1*. Accessed: Nov. 2019. [Online]. Available: https://youtu.be/pUq4r48p6Sg

[39] *Video of Scenario 2*. Accessed: Nov. 2019. [Online]. Available: https://youtu.be/M8x9WTgaDU4

[40] *Video of Scenario 3*. Accessed: Nov. 2019. [Online]. Available: https://youtu.be/4FmDKrHC9rc